catalysts

MDPI

Article

Mechanistic Insight into the 2° Alcohol Oxidation Mediated by an Efficient Cu^{I}/L-Proline-TEMPO Catalyst—A Density Functional Theory Study

Siyu Li [1], Lin Cheng [1,*], Qi Wu [2], Qiancheng Zhang [1], Jucai Yang [1] and Juming Liu [1,*]

[1] College of Chemical Engineering, Inner Mongolia University of Technology, Inner Mongolia Key Laboratory of Theoretical and Computational Chemistry Simulation, Hohhot 010051, China; lisisi1024@aliyun.com (S.L.); jzhang@imut.edu.cn (Q.Z.); yangjc@imut.edu.cn (J.Y.)

[2] High Performance Computing Center of Jilin University, Changchun 130022, China; wuqi@jlu.edu.cn

* Correspondence: lcheng1983@aliyun.com (L.C.); liujuming@imut.edu.cn (J.L.); Tel.: +86-0471-6575722 (L.C.)

Received: 10 August 2017; Accepted: 31 August 2017; Published: 5 September 2017

Abstract: Density functional theory (DFT) calculations have been performed to investigate the 2° alcohol oxidation to acetophenone catalyzed by the Cu^{I}/L-Proline-2,2,6,6- tetramethylpiperidinyloxy (TEMPO) catalyst system. Seven possible pathways (paths A→F) are presented. Our calculations show that two pathways (path A and path B) are the potential mechanisms. Furthermore, by comparing with experimental observation, it is found that path A—in which substrate alcohol provides the proton to $^{-}O^{t}Bu$ to produce $HO^{t}Bu$ followed by the oxidation of substrate directly to product acetophenone by O_2—is favored in the absence of TEMPO. Correspondingly, path B is likely to be favored when TEMPO is involved. In path B, the O–O bond cleavage of Cu^{I}–OOH to Cu^{II}–OH species occurs, followed by acetophenone formation assisted by ligand $(L)^{2-}$. It is also found that the cooperation of ligand $(L)^{2-}$ and TEMPO plays an important role in assisting the formation of the product acetophenone in path B.

Keywords: alcohol oxidation; reaction mechanism; density functional theory; aerobic oxidation; energetic span model

1. Introduction

Selective alcohol oxidation to the corresponding carbonyl product is among the most important and common transformations in organic chemical synthesis [1,2]. Recently, extensive investigations for aerobic alcohol oxidation have been focused on the design of environmentally friendly oxidation catalysts [3,4]. During the past few decades, many of the developed catalysts for aerobic alcohol oxidation are noble metal complexes, such as Pd [5–7], Au [8–10] and Ru [11–14] complexes, etc. However, by considering the limitations on the synthetic scope of these systems and their rarity, their potential uses in large-scale applications are limited. Recently, a class of copper-based catalysts has emerged as highly effective catalysts for aerobic alcohol oxidation [15–22]. However, these Cu-based catalysts usually show efficient activity for primary alcohol (1° alcohol), but the activity for secondary alcohol oxidation (2° alcohol) is unsatisfactory. Until now, only a few groups have developed Cu-based catalysts for the aerobic oxidation of 2° alcohols [23–29]. Meanwhile, the ligands for most of the reported Cu-based catalysts are confined to 1,10-phenanthroline (Phen), 2,2′-bipyridine (bipy) and their derivatives. For instance, Markó and co-workers have developed the catalyst (phen)CuCl and co-catalyst dialkylazodicarboxylates which are used to oxidize a wide range of 1° and 2° benzylic, allylic, and aliphatic alcohols [23,24]. Another copper-catalyzed 2° alcohol oxidation catalyst, introduced by Knochel and co-workers [25], utilizes a fluoroalkyl-substituted bipyridyl ligand with CuBr-Me_2S as a catalyst in a fluorous biphasic system. Recently, a highly effective catalyst system

reported by Stahl et al. made breakthroughs in aerobic alcohol oxidation [26–28]. This catalyst system [26], which features a Cu^{I} salt in combination with 4,4′-dimethoxy-2,2′-bipyridine (MeObipy), *N*-methyl-imidazole (NMI) and 9-Azabicyclo[3.3.1]nonane *N*-Oxyl (ABNO), mediates aerobic oxidation of all classes of alcohols (including 1° and 2° allylic, benzylic, and aliphatic alcohols) with nearly equal efficiency. Although most of these catalysts are efficient for 2° alcohols oxidation, the limited type of ligands for the Cu-based catalysts limit the development on the design of more efficient catalyst systems.

Fortunately, Ding and coworkers reported a Cu^{I}/L-Proline-2,2,6,6-tetramethylpiperidinyloxy (TEMPO) catalyst (L-proline: N,O-didentate ligand; commercially available and inexpensive), which has high activity in the aerobic oxidation of 2° alcohols under mild conditions [29]. It should be pointed out that this catalyst system could also catalyze 2° alcohol oxidation without TEMPO, though with less efficiency. Therefore, the Cu^{I}/L-Proline-TEMPO catalyst system is expected to be very attractive. Although Ding and coworkers have proposed a plausible mechanism based on the related studies reported by Stahl's group, a deep understanding and a clear description of the reaction pathways are still missing. Moreover, mechanistic insight of Cu^{I}/TEMPO-mediated alcohol oxidation has been the subject of debate. Three of the most prominent mechanistic proposals for the Cu^{I}-TEMPO catalyst system are depicted in Scheme 1. (1) Sheldon and co-workers presented a reaction mechanism in which one TEMPO assists the formation of the Cu^{II} center, and the second TEMPO coordinated to the Cu^{II} center plays the same role as a coordinated tyrosine radical in the galactose oxidase mechanism (Scheme 1, Sheldon) [30]; (2) Stahl et al. reported a mechanism featuring two separate half-reactions: (a) catalyst oxidation by O_2; (b) alcohol oxidation mediated by Cu^{II} and TEMPO (Scheme 1, Stahl) [31,32]; (3) In contrast to Stahl's proposals, Brückner et al. proposed a modified reaction mechanism (Scheme 1, Brückner) [33]. They found TEMPO is postulated to stabilize active (bpy)(NMI)Cu^{II}-$O_2^{\bullet -}$-TEMPO species. Besides the uncertain mechanism, understanding the role of the L-proline ligand in the catalytic cycle could also be beneficial in providing useful information for developing new ligands to assist the alcohol oxidation reaction. Herein, we present DFT calculations for the Cu^{I}/L-Proline-TEMPO catalyst system. We hope the investigation of the catalytic reaction mechanism will provide useful insight for the development of new synthetic aerobic oxidation catalysts.

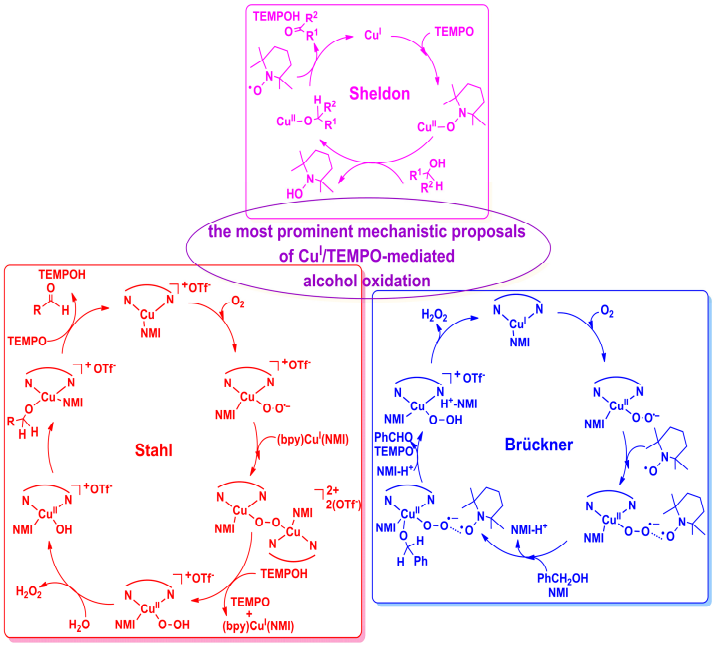

Scheme 1. Three prominent mechanistic proposals for the Cu^{I}/2,2,6,6-tetramethylpiperidinyloxy (TEMPO)-mediated alcohol oxidation reaction.

2. Results and Discussion

2.1. Reaction Models

Since Ding and co-workers selected 1-phenethyl alcohol as the model substrate to determine the optimal condition in Ref. [29], 1-phenethyl alcohol was selected to represent 2° alcohol in this work. Under the optimal reaction condition (1.0 mmol alcohol, 5 mol % TEMPO, 1.0 equiv ^{t}BuOK, 5 mol % Cu^{I}, 5 mol % L-proline), Ding and co-workers demonstrate that L-proline is in its deprotonated form (denoted as $(L)^{2-}$ in the following discussion) under alkaline conditions, and this ligand $(L)^{2-}$ coordinates to Cu^{I} ion to form the $(L)^{2-}$-ligated Cu^{I} species. On the basis of the reaction mechanisms proposed by Stahl et al. [31,32], Brückner et al. [33] and Sheldon et al. [30], two Cu^{I} complexes bearing ligand $(L)^{2-}$ were considered as the probable catalyst models (Model A: $[(L)^{2-}(Cu^{I})(^{-}O^{t}Bu)]^{2-}$(**0**); Model B: $[(L)^{2-}Cu(TEMPO)]^{-}$(**^{2}29**)).

2.2. Possible Reaction Mechanisms

2.2.1. Catalyst Model A

Starting from complex $[(L)^{2-}(Cu^{I})(^{-}O^{t}Bu)]^{2-}$(**0**), six pathways (paths A→E) are explored (Scheme 2). Among them, path A, path B and path B′ are proposed in this work, while paths C→E are proposed on the basis of the reaction mechanisms presented by Stahl et al. [31,32], Brückner et al. [33] and Ding et al. [29], respectively. As seen in Scheme 2, in process **^{1}0**→**^{1}4**, the product acetophenone is formed by the assistance of oxygen. Subsequently, three pathways (Paths A, B and B′) from **^{1}4** are explored. Path A proceeds through the replacement of the product acetophenone by substrate $PhCH(OH)CH_3$. While in path B and B′, TEMPOH and TEMPO are used to replace the product acetophenone.

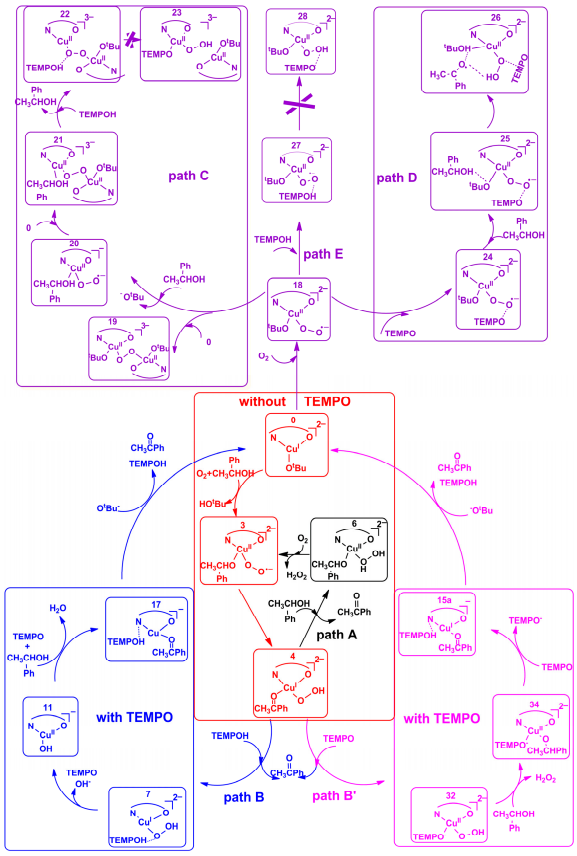

Scheme 2. Six possible reaction mechanisms for model A, i.e., Paths A→E.

- Formation of Product Acetophenone in Process ^{1}**0**→^{1}**4**

From **0**, coordination of substrate PhCH(OH)CH_3 to **0** gives **1** ([$(L)^{2-}$(Cu^{I})(PhCH(OH)CH_3)($^{-}$O^{t}Bu)]$^{2-}$). Next, a proton migration from substrate alcohol to $^{-}$O^{t}Bu species generates **2** ([$(L)^{2-}$(Cu^{I})(PhCH(O^{-})CH_3)(HO^{t}Bu)]$^{2-}$). The energy barrier for this proton transfer process, ^{1}**1**→^{1}**TS$_{1-2}$**, is 17.7 kcal/mol (Figure 1). Subsequently, the weakly coordinated closed-shell singlet HO^{t}Bu molecule is replaced by open-shell triplet O_2 to generate **3** in a singlet (^{1}**3**, S = 0) and triplet (^{3}**3**, S = 1) states. In ^{3}**3**/^{1}**3**, the spin populations on Cu center, O_2 species, PhCH(O^{-})CH_3 and ligand $(L)^{2-}$ are +0.51/+0.53, +1.13/−0.90, +0.10/+0.09, and +0.26/+0.28, respectively. These data indicate that ^{3}**3**/^{1}**3** possess the [$(L)^{2-}$(PhCH(O^{-})CH_3)Cu^{II}($OO^{\bullet-}$)]$^{2-}$ character. In the following step, the $OO^{\bullet-}$ species abstracts the H atom from the C_α–H bond of PhCH(O^{-})CH_3 moiety (**3**→**4** in Figure 1). As seen in Figure 1, this H abstraction step involves a spin crossover from the S = 1 ground state to the S = 0 transition state (^{1}**TS$_{3-4}$**). Therefore, the minimum energy crossing point (MECP) is calculated by MECP program [34–36]. An accurate structure of MECP is located as **3′-MECP** (ΔE = 12.3 kcal/mol). Through **3′-MECP**, ^{3}**3** crosses to the singlet potential energy surface leading to ^{1}**4** ([$(L)^{2-}$)(PhC(O)CH_3)Cu^{I}(OOH)]$^{2-}$). After ^{1}**4**, three pathways (paths A, B and B′) are explored.

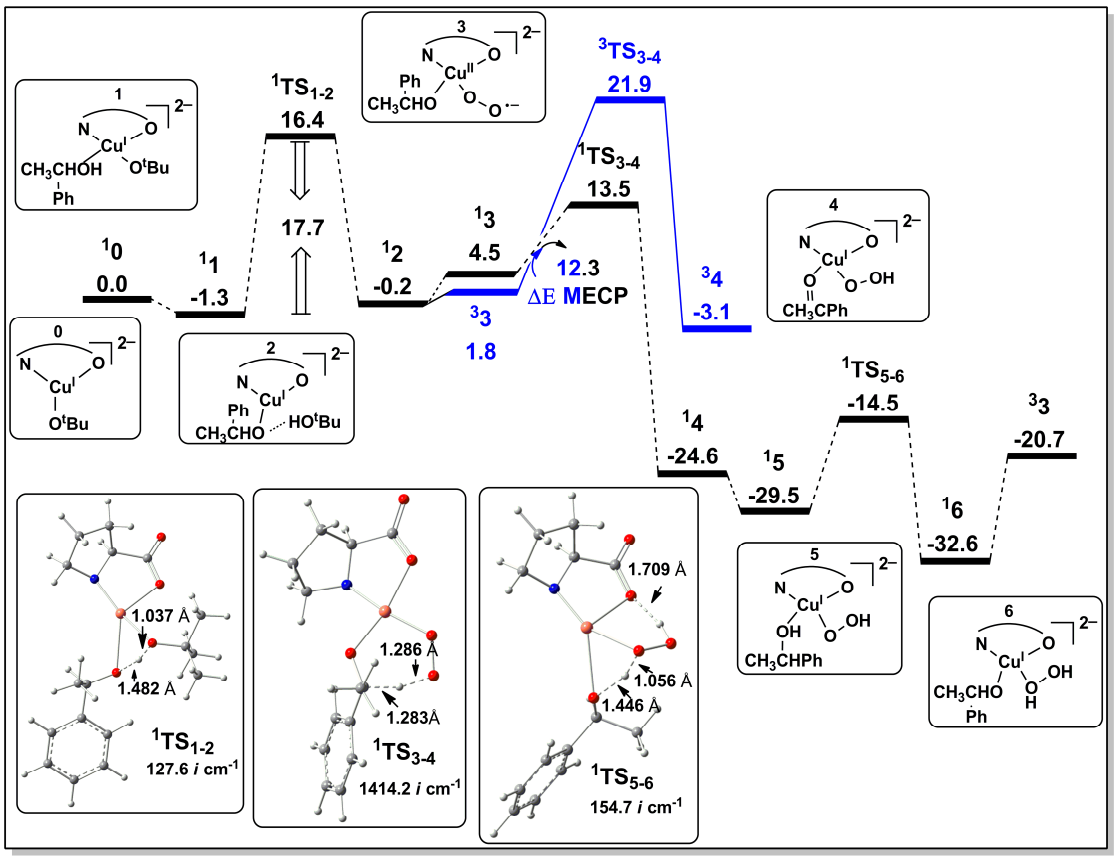

Figure 1. The calculated Gibbs free energy profiles for process **0**→**4** and path A. The solid blue line represents the triplet spin state; the dashed black line represents the singlet state. The energy values are in kcal/mol.

- Path A

In path A, after ^{1}**4**, the product acetophenone is hereby replaced by PhCH(OH)CH_3 to form ^{1}**5** (Figure 1). Then, the proton migrates from PhCH(OH)CH_3 to –OOH moiety to give ^{1}**6** ([$(L)^{2-}$(PhCH(O)CH_3)Cu^{I}(H_2O_2)]$^{2-}$). Finally, H_2O_2 is replaced by O_2 to regenerate **3** to finish the catalytic cycle. To assess the efficiency of the catalytic cycle in path A, the energetic span

model introduced by Kozuch and Shaik [37–41] was used to identify the Turnover Frequency (TOF)-determining intermediate (TDI) as ^{1}**6** and the TOF-determining transition state (TDTS) as ^{1}**TS$_{3-4}$**, corresponding to an energy span (δE) of 23.6 kcal/mol (calculated by AUTOF program [37–41], based on the theoretically obtained energy profile in Figure 1). Moreover, it is noted that TEMPO was not involved in the catalytic cycle in path A. Thus, path A is likely the favorable pathway for the Cu^{I}/L-Proline-TEMPO catalyst system without TEMPO.

- Path B

1. TEMPO or TEMPOH (1-Hydroxy-2,2,6,6-tetramethylpiperidine) coordination?

From ^{1}**4**, another two pathways are designed (path B and path B′ in Scheme 2). The product acetophenone is replaced by TEMPO in path B′, while replaced by TEMPOH in path B. The calculated results show that path B′ should be excluded for the fairly high energetic span (δE = 55.7 kcal/mol, Figure S1 in the Supplementary Materials). The high energetic span for path B′ could trace to the sterically sensitive TEMPO. Stahl and coworkers demonstrate that steric effects of the nitroxyl radical have a key influence on their reactivity toward alcohol oxidation [26,34]. Therefore, direct binding of TEMPO to Cu center in path B′ (^{2}**32**→^{2}**34**) is likely to be more susceptible to steric hindrance than path B (^{1}**7**→^{1}**10**), where interaction occurs at the second coordination sphere of Cu center. Thus, only path B is discussed below.

As we know, there is no TEMPOH adding to the catalytic system at the beginning of the reaction. In finding where TEMPOH comes from, we speculate that the origin of TEMPOH likely comes from path F at the beginning of the reaction (details in Section 2.2.2). As the reaction goes on, the catalyst is consumed and the concentration of TEMPOH ([TEMPOH]) increases. When [TEMPOH] reaches a certain concentration, path B would be initiated. Then, TEMPOH replaces the product acetophenone to form two isomers ^{1}**7** and ^{1}**7′** (Scheme 3). In ^{1}**7**, the proton on TEMPOH forms a hydrogen bond with the proximal oxygen atom of the Cu^{I}–OOH species, while in ^{1}**7′**, TEMPOH is hydrogen-bonded to the distal oxygen. It is found that ^{1}**7** is 7.5 kcal/mol lower than ^{1}**7′**. Subsequently, the formation of either complex ^{1}**8** or complex ^{1}**35** from ^{1}**7** to ^{1}**7′** (Scheme 3) was computed. The formation of ^{1}**8** from ^{1}**7** requires overcoming an energy barrier that is 1.4 kcal/mol higher than forming ^{1}**35** from ^{1}**7′**. These results indicate that the formation of ^{1}**8** is energetically more favorable than the formation of ^{1}**35**. Thus, only the favorable pathway from ^{1}**7** is discussed below. The corresponding energy profile is shown in Figure 2. Detailed information for the pathway from ^{1}**7′** is collected in Supplementary Materials (Figure S2).

2. Formation of Cu–OH Species

In process ^{1}**7**→^{1}**8**, TEMPOH could assist the homolysis or heterolysis of the O–O bond in the Cu^{I}–OOH moiety to form either Cu^{II}=O and $^{\bullet}$OH or a Cu^{III}–O^{2-} and $^{-}$OH. Thus, the closed singlet and open shell singlet potential energy surfaces in process ^{1}**7**→^{1}**8** are explored. It is found that the open shell singlet ^{1u}**TS$_{7-8}$** converges to the closed singlet ^{1}**TS$_{7-8}$** during the optimization process. This result demonstrates that TEMPOH assists the heterolytic cleavage of the O–O bond of Cu^{I}–OOH moiety. To get clearer insight into this O–O bond cleavage, changes in the electronic structure from ^{1}**7** to ^{1}**8** are examined. The results show that the electronic configurations of Cu center in ^{1}**7** is $d^{2}_{yz}d^{2}_{z2}d^{2}_{xz}d^{2}_{xy}d^{2}_{x2-y2}$, indicating the Cu^{I} oxidation state, while that in ^{1}**8** is $d^{2}_{yz}d^{2}_{z2}d^{2}_{xz}d^{2}_{xy}d^{0}_{x2-y2}$, implying the Cu^{III} oxidation state. This result further supports the heterolytic cleavage of the O–O bond. Moreover, Wiberg Bond Index (WBI) is calculated by Multiwfn program [42]. It is found that, as the O–O bond is weakened, the O–Cu bond is strengthened in process ^{1}**7**→^{1}**TS$_{7-8}$**→^{1}**8** (O–O: 1.30→0.13→0.00; O–Cu: 0.87→1.60→1.72). This is further verified by the bond length variations for the O–O and O–Cu bonds (O–O: 1.495 Å→3.069 Å→8.172 Å; O–Cu: 1.878 Å→1.712 Å→1.685 Å). Thus, in process ^{1}**7**→^{1}**8**, the heterolytic cleavage of the O–O bond generates the Cu^{III}–O^{2-} moiety and $^{-}$OH species. Subsequently, $^{-}$OH species dissociate, followed by the H atom transfer from TEMPOH to Cu^{III}–O^{2-} species to form Cu^{II}–OH species and TEMPO (^{1}**8**→^{1}**10**). After ^{1}**10**, dissociation of TEMPO

results in the formation of Cu^{II}–OH species (^{2}**11**). This Cu^{II}–OH species has been reported as the active species in Stahl's catalyst system (Cu^{I}(OTf)-TEMPO) [32].

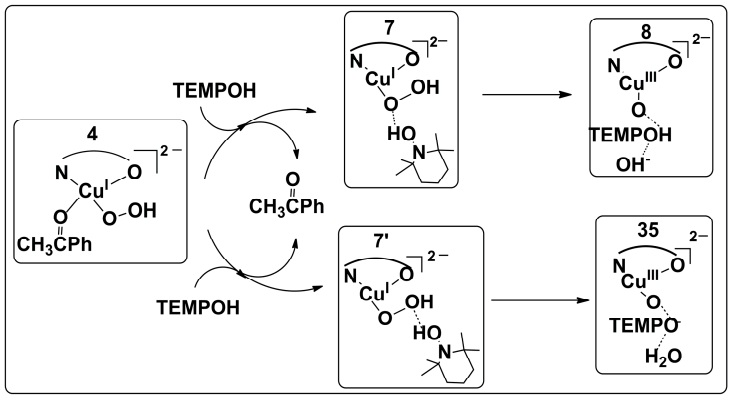

Scheme 3. Two probabilities for 2,2,6,6-tetramethylpiperidinyloxy (TEMPO) coordination.

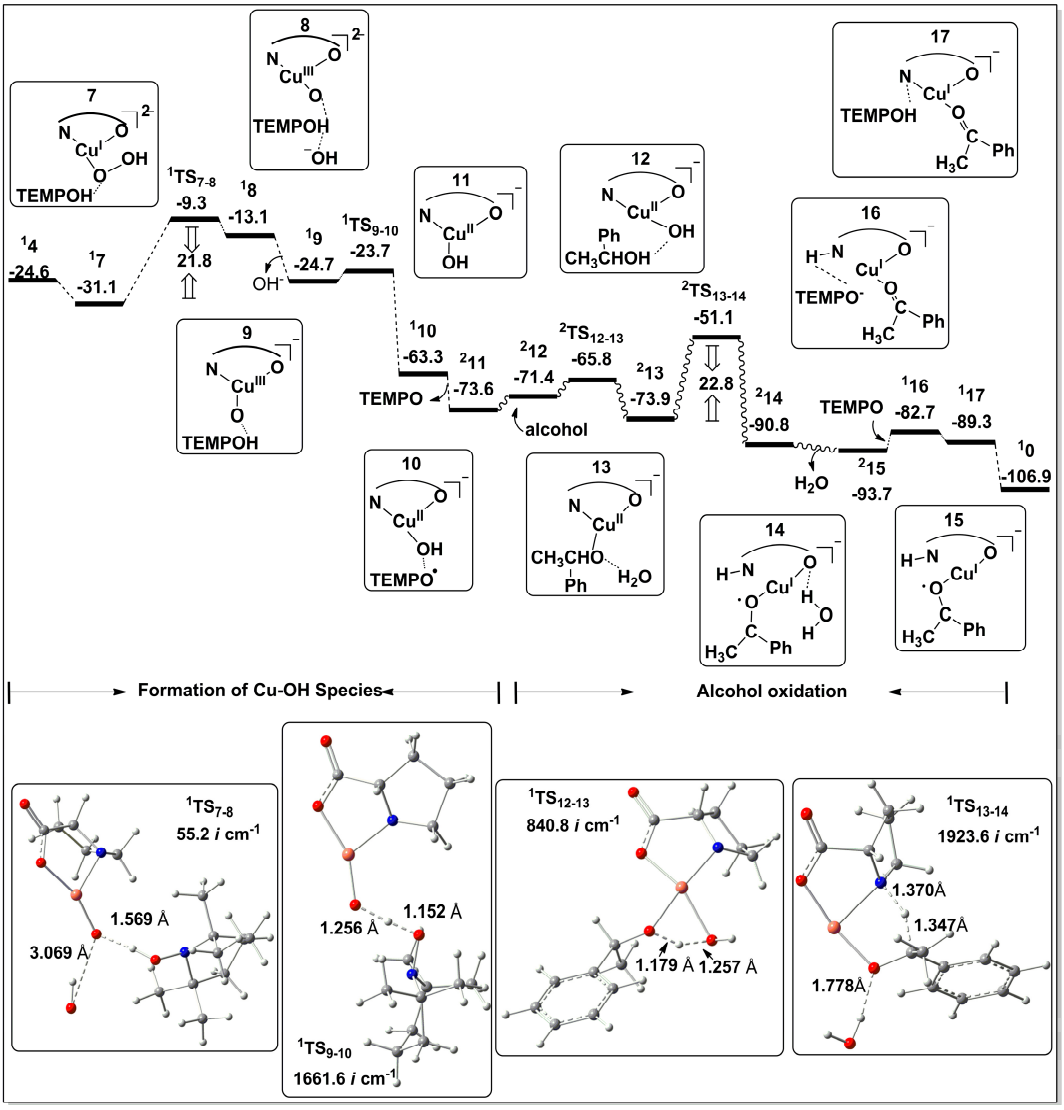

Figure 2. The calculated Gibbs free energy profiles for path B. The dashed line represents the singlet state; the wave line represents the doublet state. The energy values are in kcal/mol.

3. Alcohol Oxidation

In the following steps (**^{2}11**→**^{2}13**), a proton transfers from substrate $PhCH(OH)CH_3$ to ^-OH moiety to form a Cu–alkoxide adduct **^{2}13** ($[(L^{2-})Cu^{II}(PhCH(O^-)CH_3)(H_2O)]^-$). From **^{2}13**, the singlet H_2O molecule is replaced by doublet TEMPO to generate **14a** in singlet (**^{1}14a**) and triplet (**^{3}14a**) (Figure S3). Then, the H atom transfers from alkoxide either to the oxygen atom of η^1-TEMPO via **$TS_{14a\text{-}15a\_O}$** or to the unbound nitrogen atom of η^1-TEMPO via **$TS_{14a–15a\_N}$** (identified by Baerends et al. [43,44]. and Stahl et al. [32]). The calculated energy barriers for both pathways are >28.7 kcal/mol (**$TS_{14a\text{-}15a\_N}$**/**$TS_{14a\text{-}15a\_O}$** relative to **^{2}13** in Figure S3). These data indicate that the C_α–H bond activation step might not be assisted by TEMPO. Then, the question is what assists this step. To answer this question, let us to gain insight into the electronic structure of **^{2}13**. The molecular orbital for **^{2}13** illustrates that one unpaired electron is located in Cu $d_{x2\text{-}y2}$ orbital (29.2% Cu character) with a significant contribution of P_z orbital of the $N_{(L)2^-}$ atom (34.3% N character) (Scheme 4). This result suggests that the $N_{(L)2^-}$ atom could abstract the H atom from alkoxide. The corresponding activation barrier for this H atom transfer is 22.8 kcal/mol (Figure 2). Therefore, instead of TEMPO, ligand $(L)^{2-}$ assists the C_α–H bond activation. However, product acetophenone is not formed in process **^{2}13**→**^{2}14**. In **^{2}14**, the spin populations are +0.00 on Cu, +0.00 on ligand $(L)^{2-}$, and +1.00 on $PhC(O)CH_3$ moiety, implying the $[(HL^{2-})Cu^{I}(PhC(O^\bullet)CH_3)(H_2O)]^-$ character. Thus, another oxidized agent must be needed to give the product acetophenone. In this case, TEMPO is supposed to assist the formation of acetophenone (**^{1}16**→**^{1}17**). Finally, $^-O^tBu$ species replace TEMPOH and acetophenone to reproduce **0** to close the catalytic cycle. Obviously, TEMPO and ligand $(L)^{2-}$ act together to assist the formation of product acetophenone. The efficiency of the catalytic cycle in path B was also assessed by the AUTOF program. The results identify **^{2}13** as TDI and **$^2TS_{13–14}$** as TDTS, corresponding to an energetic span (δE) of 22.8 kcal/mol. Since TDI and TDTS are the key factors affecting TOF [37], the electron transfer process during **^{2}13**→**$^2TS_{13–14}$** is discussed. The spin population on Cu center decreases from +0.41 to +0.06 (**^{2}13**→**$^2TS_{13–14}$**), illustrating that a fraction of β-electron has been migrated to Cu center. This fraction of β-electron comes from the homolytic cleavage of the Cu–$N_{L2_}$ bond. The corresponding α-electron migrates to ligand $(L)^{2-}$ (especially to $N_{L2\_}$ atom), which should result in the increase of α-spin populations on ligand $(L)^{2-}$. However, it is noted that the spin population on ligand $(L)^{2-}$ decreases from +0.57 to +0.47. This change is related to the homolytic cleavage of C_α–H bond of substrate. The C_α–H bond homolytic cleavage could give a fraction of β-spin electron to ligand $(L)^{2-}$, to make the α-spin population on ligand $(L)^{2-}$ decrease to +0.47. The corresponding α-electron migrates to the substrate to make the α-spin population on the substrate increase from +0.03 to +0.53 in the process **^{2}13**→**$^2TS_{13–14}$**. Therefore, two bonds (Cu–$N_{L2_}$ and C_α–H bonds) are partially in homolytic cleavage in the process **^{2}13**→**$^2TS_{13–14}$**. This conclusion is further verified by WBI analysis. The results show that the Cu–$N_{L2_}$ and C_α–H bonds are weakened (55% of Cu–$N_{L2\_}$ and 45% of C_α–H bonds are broken at **$^2TS_{13–14}$**), while the Cu–O_{sub} bond remains (Table 1). Meanwhile, the bond length variations for the Cu–$N_{L2\_}$ and C_α–H bonds in process **^{2}13**→**$^2TS_{13–14}$** (Cu–$N_{L2_}$: 1.871 Å→2.189 Å; C_α–H: 1.104 Å→1.347 Å) are observed as well.

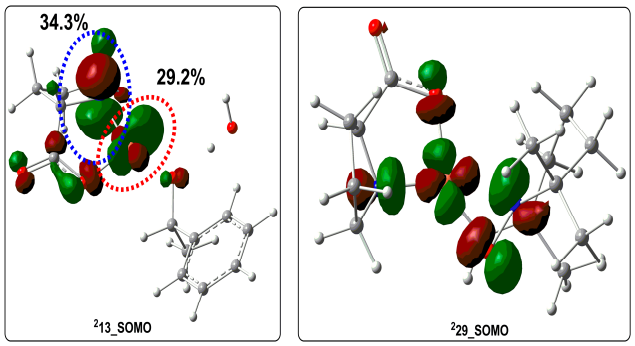

Scheme 4. Molecular orbital diagram for **^{2}13** and **^{2}29**. (Contour values = ±0.05).

Table 1. Distances and Wiberg Bond Index (WBI) for Cu–N_{L2-}, C_α–H and Cu–O_{sub} for ^{2}**13** and ^{2}**TS$_{13–14}$**.

Structures	Cu–N_{L2-}	C_α–H	Cu–O_{sub}	Cu–N_{L2-} (WBI)	C_α–H (WBI)	Cu–O_{sub} (WBI)	Cu–N_{L2-} Formed %	C_α–H Formed %	Cu–O_{sub} Formed %
^{2}**13**	1.871 Å	1.104 Å	1.888 Å	1.037	0.823	0.828	100	100	100
^{2}**TS$_{13–14}$**	2.189 Å	1.347 Å	1.892 Å	0.466	0.451	0.789	44.9	54.8	95.3

- Path C

Path C is suggested based on the reaction mechanism disclosed by Stahl and co-workers (Scheme 2). The computed Gibbs free-energy profile is provided in Figure S4. Initially, oxidation of **0** with oxygen gives ^{3,1}**18**. For ^{3}**18** (^{1}**18**), calculated spin populations on Cu, O_2 species and ligand $(L)^{2-}$ are +0.46 (+0.52), +1.22 (−0.85) and +0.25 (+0.27), respectively, implying the Cu^{II}–$OO^{\bullet-}$ character. Then, we suppose that another **0** coordinates to ^{3,1}**18** to form a binuclear Cu^{II} species Cu_2O_2 (**19**). For **19**, three dominant bonding motifs are considered (side-on μ-η^2:η^2-peroxo, bis-μ-oxo-Cu^{III} and trans end-on μ-η^1:η^1-superoxo) [45]. However, all the efforts to locate the binuclear Cu^{II} species failed. They all dissociate to **0** and **18** during the optimization. Therefore, another possibility is discussed. From **18**, $^{-}O^{t}Bu$ moiety is replaced by $PhCH(OH)CH_3$ to form **20**, followed by another **0** coordination to form **21**. Nonetheless, the formation of **21** is endothermic 29.0 kcal/mol. Clearly, such a complex **21** is unfavorable to be formed. Moreover, the transition state ^{3}**TS$_{22–23}$** in the following H migration process from TEMPOH to Cu–$OO^{\bullet-}$ moiety is not located in our work. Thus, path C should be ruled out.

- Path D

Path D is suggested based on the reaction mechanism reported by Brückner et al. (Scheme 2). From **18**, TEMPO initially coordinates to form **24**. This step is endothermic by 19.6 kcal/mol (Figure S5), meaning **24** is unfavorable to be generated. Even if **24** is formed, the activation energy barrier for the following concerted step (^{3}**25**→^{3}**TS$_{25–26}$**) is still high for a reaction occurring at room temperature (51.1 kcal/mol; ^{3}**TS$_{25–26}$** relative to ^{1}**0** in Figure S5). Thus, path D should also be excluded.

- Path E

Path E is suggested based on the reaction mechanism reported by Ding and co-workers (Scheme 2). From ^{3}**18**, TEMPOH comes to **18** to form a hydrogen bond to O atom of Cu^{II}–$OO^{\bullet-}$ moiety in ^{3}**27**. This initial step is endothermic by 13.7 kcal/mol. Then, TEMPOH gives an H atom to the Cu^{II}–$OO^{\bullet-}$ moiety to form Cu^{II}–OOH and TEMPO (**28**). However, all the efforts to locate the transition state **TS$_{27–28}$** and intermediate **28** failed; they all come back to **27** during the optimization. Therefore, this pathway should be ruled out as well.

As a result, for catalyst model A, path B′, path C, path D and path E are not preferred. Path A and path B are the possible routes (details in Section 2.2.3).

2.2.2. Catalyst Model B

For catalyst model B, path F is explored. Path F is proposed based on Sheldon's mechanism [30]. The corresponding energy profiles and optimized structures are illustrated in Figure 3. In path F, the starting structure is $[(L^{2-})Cu(TEMPO)]^{-}$ (^{2}**29**), and two possible binding motifs ($[(L^{2-})Cu^{II}(TEMPO^{-})]^{-}$ or $[(L^{2-})Cu^{I}(TEMPO^{\bullet})]^{-}$) were taken into account. The calculated singlet occupied molecular orbital for ^{2}**29** is shown in Scheme 4. Obviously, the unpaired electron is located on Cu d_{x2-y2} orbital with a significant contribution of the σ orbital of the connecting atoms. This spin distribution explains the α-spin populations on TEMPO (+0.33) and L-Proline (+0.22). In addition, the O–N bond length of TEMPO group is 1.413 Å in ^{2}**29**, consistent with the 1.410 Å in $TEMPO^{-}$ anion (1.285 Å in TEMPO radical). Combining the above results, it is obvious that ^{2}**29** is in the $[(L^{2-})Cu^{II}(TEMPO^{-})]^{-}$character.

Subsequently, the addition of $PhCH(OH)CH_3$ to ^{2}**29** leads to the formation of ^{2}**30**. From ^{2}**30**, the following step is proton migration from $PhCH(OH)CH_3$ to $TEMPO^-$ anion to form TEMPOH via ^{2}**TS$_{30–31}$** (19.4 kcal/mol relative to ^{2}**29**). Thus, TEMPOH species generating from ^{2}**29**→^{2}**31** in path F would be the origin of the TEMPOH species at the beginning of the reaction. In the following step, replacing TEMPOH by TEMPO leads to ^{2}**14a**, followed by an H atom abstraction step (**14a**→**15a**). The energy barrier for this H abstraction step is 41.4 kcal/mol, which is fairly high for a reaction occurring at room temperature. Thus, path F should be excluded as well.

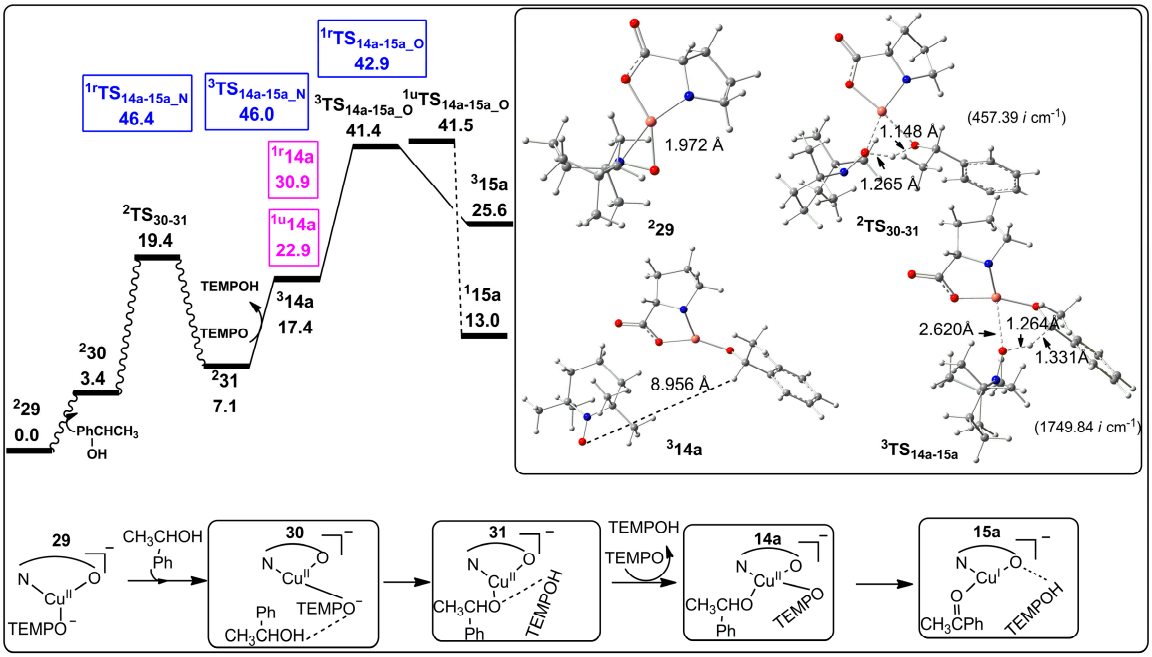

Figure 3. The calculated Gibbs free energy profiles and the optimized geometries for path F. The dashed line represents the singlet state; the solid blue line represents the triplet spin state; the wave line represents the doublet state. The energy values are in kcal/mol.

2.2.3. Preliminary Mechanistic Assessment

Overall, the three previous prominent mechanistic proposals (paths C, D and F) presented by Stahl et al. [31,32], Brückner et al. [33], Sheldon et al. [30] and Ding's mechanistic proposal (path E) are not preferred. For path A and path B, the energy spans are 23.6 kcal/mol and 22.8 kcal/mol, respectively, indicating that both pathways are possible routes. Experimentally, Ding and coworkers demonstrate that this Cu^I/L-Proline-TEMPO catalyst system could catalyze 2° alcohols without TEMPO. Thus, based on the aforementioned calculation results, path A would be the main route when TEMPO is not involved in this catalyst system. Then the question arises: which pathway is the dominant reaction pathway for this catalyst system in the presence of TEMPO? We tentatively assign path B as the dominant pathway for this Cu^I(L-Proline)/TEMPO-mediated alcohol oxidation reaction. Our preliminary explanations are as follows: (1) One can see that the energy span of path A (23.6 kcal/mol) is 0.8 kcal/mol higher than that of path B (22.8 kcal/mol); (2) The formation of ^{1}**7** in path B is found to be more favorable than the formation of ^{1}**5** in path A (Figure 2). Meanwhile, ^{1}**7** can be transferred to ^{2}**11** via a high exergonicity of the process (**7**+TEMPOH→**11**+TEMPO). This might deplete ^{1}**7** very fast and thus reduce the probability of the formation of ^{1}**5**; (3) Ding and coworkers found that the conversion of product increases from 10% (TEMPO-free) to >99% (with TEMPO). This experimental observation shows that TEMPO should be involved in the catalytic cycle. Thus, path B is likely to be the dominant pathway for this Cu^I/L-Proline-TEMPO catalyst system and the cooperation of ligand $(L)^{2-}$ and TEMPO plays an important role in assisting the formation of the product acetophenone.

In a word, although we can tentatively assign path B as the dominant pathway for the Cu^{I}/L-Proline-TEMPO catalyst system, more evidence is clearly necessary. For the case without TEMPO, path A is the main route.

3. Computational Details

All the calculations were carried out with the Gaussian 09 series of programs [46]. The B3LYP [47–49] functional with a standard 6-31+G(d) basis set was used for geometry optimizations in gas phase, and frequency calculations were carried out at the same level of theory. The intrinsic reaction coordinate (IRC) approach was used to confirm that the transition state connects the two relevant minima [50,51]. The combination of using B3LYP for geometry optimizations and M06 for single point calculations has been successfully applied to investigate various transition metal-catalyzed reactions [52–64], including organocopper systems [60–64]. Thus, to further refine the energies, single-point energy calculations were performed on the stationary points at M06/6-311+G(d,p) level [65,66] with the SMD solvation model [67] and *N*,*N*-Dimethylformamide (DMF) as the solvent using the gas-phase optimized structures. For comparison purposes, the key intermediates and transition states were subject to reoptimization with B3LYP/6-31+G(d)/SMD(DMF) and single-point energy calculations with M06/6-311+G(d,p)/SMD(DMF), and the outcomes were consistent with the M06/6-311+G(d,p)/SMD(DMF)//B3LYP/6-31+G(d) results (Table S1A in the Supplementary Materials). Spin populations are reported by Mulliken population analysis from single-point energy calculations. Geometrical counterpoise correction and the dispersion correction were also calculated by using gCP program and DFT-D3 program of Grimme [68–72]. To ensure our conclusions are not affected by the choice of the computational method used in this study, the key intermediates and transition states were recalculated with different DFT methods. According to benchmarking research [73,74], two commonly used modern functionals—the nonlocal hybrid meta GGA TPSSh [75] and Wb97xd [76] (including empirical dispersion)—were tested. These test calculations show that the relative energetic spans between the competing pathways are not affected by the choice of methods (Table S1B in the Supplementary Materials). In addition, the MECP in this work was located with the code developed by Harvey and co-workers at the B3LYP/6-31G(d) level [34–36] and only the electronic energy (ΔE) was evaluated at the M06/6-311+G(d,p)/SMD(DMF)//B3LYP/6-31G(d) level. Some open-shell calculations for the anti-ferromagnetic coupled singlet state resulted in a degree of spin contamination. Therefore, an energy correction was estimated from the Heisenberg spin-Hamiltonian formalism [77–79]. A similar energy correction approach was used in previous studies [80–83]. Detailed cartesian coordinates and corrections to Gibbs free energies for each reported structures have been presented in Tables S2 and S3.

4. Conclusions

We have studied the reaction mechanisms for the oxidation of 1-phenethyl alcohol to the corresponding acetophenone by Cu^{I}/L-Proline-TEMPO catalyst system by use of the density functional method. Seven pathways (paths A→F) in models A and B were presented. The kinetic assessments based on the Energetic Span Model are used to discriminate the possible pathways. The calculated results show that three previous prominent mechanistic proposals (paths C→F) and Ding's proposal (path E) are excluded as possible mechanisms for the Cu^{I}/L-Proline catalyst system. Instead, two new reaction mechanisms (path A and path B) are presented. The calculated energy spans of path A and path B are 23.6 kcal/mol and 22.8 kcal/mol, respectively. In combination with the experimental result, we suppose that both pathways (path A and path B) are possible routes. Path B is likely to be the dominant catalytic cycle for the Cu^{I}/L-Proline-TEMPO catalyst system. In contrast, path A is supposed to be the main route for the case without TEMPO. Besides, by further investigation into alcohol oxidation part in path B, it is found that TEMPO is not directly involved in the C_{α}–H bond cleavage of $PhCH(O^{-})CH_3$ moiety in the TOF determining Transition State (**$TS_{13–14}$**). Instead, ligand

$(L)^{2-}$ actually acts as the H atom sink to locate the H atom of the C_{α}–H bond in the $PhCH(O^{-})CH_3$ moiety in TDTS $\mathbf{TS_{13-14}}$ and TEMPO assists the formation of the product acetophenone.

Supplementary Materials: The following are available online at www.mdpi.com/2073-4344/7/9/264/s1. Table S1A: Comparison of the energy barriers for processes $^{1}\mathbf{7}\rightarrow{}^{1}\mathbf{TS_{7-8}}$ and $^{2}\mathbf{13}\rightarrow{}^{2}\mathbf{TS_{13-14}}$ between the optimized structures in the gas phase and the solvent; Table S1B: Comparison of energetic spans (δE) for path A and path B at different levels of theories; Table S2: Cartesian coordinates of all structures considered in this work (B3LYP level); Table S3: Relative corrections to Gibbs free energies for each reported structures; Figure S1: The calculated Gibbs free energy profiles for path B′. The energy values are in kcal/mol; Figure S2: The calculated Gibbs free energy profiles for the process of $\mathbf{7'}\rightarrow\mathbf{44}$. The energy values are in kcal/mol; Figure S3: The calculated Gibbs free energy profiles for the process of $^{2}\mathbf{13}\rightarrow{}^{1}\mathbf{15a}$. The energy values are in kcal/mol; Figure S4: The calculated Gibbs free energy profiles for Path C. The energy values are in kcal/mol; Figure S5: The calculated Gibbs free energy profiles for Path D. The energy values are in kcal/mol.

Acknowledgments: The authors thank the National Natural Science Foundation of China (NSFC) (Grant No. 21343007, 21403117), the Natural Science Foundation of the Inner Mongolia Autonomous Region (Grant No. 2016MS0206) and Program for Innovative Research Team in Universities of Inner Mongolia Autonomous Region (NMGIRT-A1603).

Author Contributions: Lin Cheng and Juming Liu conceived and designed the experiments; Siyu Li performed the experiments; Qi Wu, Qiancheng Zhang and Jucai Yang analyzed the data; Siyu Li and Lin Cheng wrote the paper.

Conflicts of Interest: The authors declare no conflict of interest.

References

1. Parmeggiani, C.; Cardona, F. Transition metal based catalysts in the aerobic oxidation of alcohols. *Green Chem.* **2012**, *14*, 547–564. [CrossRef]
2. Tojo, G.; Fernandez, M. Oxidations Mediated by TEMPO and Related Stable Nitroxide Radicals (Anelli Oxidation). In *Oxidation of Alcohols to Aldehydes and Ketones*; Tojo, G., Ed.; Springer: New York, NY, USA, 2010; pp. 241–253.
3. Mallat, T.; Baiker, A. Oxidation of alcohols with molecular oxygen on solid catalysts. *Chem. Rev.* **2004**, *104*, 3037–3058. [CrossRef] [PubMed]
4. Schultz, M.J.; Sigman, M.S. Recent advances in homogeneous transition metal-catalyzed aerobic alcohol oxidations. *Tetrahedron* **2006**, *62*, 8227–8241. [CrossRef]
5. Brink, G.J.T.; Arends, I.W.C.E.; Sheldon, R.A. Green, Catalytic oxidation of alcohols in water. *Science* **2000**, *287*, 1636–1639. [CrossRef] [PubMed]
6. Sigman, M.S.; Jensen, D.R. Ligand-modulated palladium-catalyzed aerobic alcohol oxidations. *Acc. Chem. Res.* **2006**, *39*, 221–229. [CrossRef] [PubMed]
7. Liu, C.; Tang, S.; Lei, A.W. Oxidant controlled Pd-catalysed selective oxidation of primary alcohols. *Chem. Commun.* **2013**, *49*, 1324–1326. [CrossRef] [PubMed]
8. Guan, B.T.; Xing, D.; Cai, G.X.; Wan, X.B.; Yu, N.; Fang, Z.; Yang, L.P.; Shi, Z.J. Highly selective aerobic oxidation of alcohol catalyzed by a gold(I) complex with an anionic ligand. *J. Am. Chem. Soc.* **2005**, *127*, 18004–18005. [CrossRef] [PubMed]
9. Miyamura, H.; Matsubara, R.; Miyazaki, Y.; Kobayashi, S. Aerobic oxidation of alcohols at room temperature and atmospheric conditions catalyzed by reusable gold nanoclusters stabilized by the benzene rings of polystyrene derivatives. *Angew. Chem. Int. Ed.* **2007**, *46*, 4151–4154. [CrossRef] [PubMed]
10. Karimi, B.; Esfahani, F.K. Gold nanoparticles supported on the periodic mesoporous organosilicas as efficient and reusable catalyst for room temperature aerobic oxidation of alcohols. *Adv. Synth. Catal.* **2012**, *354*, 1319–1326. [CrossRef]
11. Dijksma, A.; Marino-Gonzalez, A.; Payeras, A.M.; Arends, I.W.C.E.; Sheldon, R.A. Efficient and selective aerobic oxidation of alcohols into aldehydes and ketones using ruthenium/TEMPO as the catalytic system. *J. Am. Chem. Soc.* **2001**, *123*, 6826–6833. [CrossRef]
12. Lenz, R.; Ley, S.V. Tetra-n-propylammonium perruthenate (TPAP)-catalysed oxidations of alcohols using molecular oxygen as a co-oxidant. *J. Chem. Soc. Perkin Trans. 1* **1997**, *1*, 3291–3292. [CrossRef]
13. Hasan, M.; Musawir, M.; Kozhevnikov, I.V. Oxidation of primary alcohols to aldehydes with oxygen catalysed by tetra-n-propylammonium perruthenate. *J. Mol. Catal. A* **2002**, *180*, 77–84. [CrossRef]

14. Mizuno, N.; Yamaguchi, K. Selective aerobic oxidations by supported ruthenium hydroxide catalysts. *Catal. Today* **2008**, *132*, 18–26. [CrossRef]
15. Semmelhack, M.F.; Schmid, C.R.; Cortes, D.A.; Chou, C.S. Oxidation of alcohols to aldehydes with oxygen and cupric ion, mediated by nitrosonium ion. *J. Am. Chem. Soc.* **1984**, *106*, 3374–3376. [CrossRef]
16. Jiang, N.; Ragauskas, A.J. Cu(II)-catalyzed selective aerobic oxidation of alcohols under mild conditions. *J. Org. Chem.* **2006**, *71*, 7087–7090. [CrossRef] [PubMed]
17. Figiel, P.J.; Sibaouih, A.; Ahmad, J.U.; Nieger, M.; Räisänen, M.T.; Leskelä, M.; Repo, T. Aerobic oxidation of benzylic alcohols in water by 2,2,6,6-tetramethylpiperidine-1-oxyl (TEMPO)/Copper(II) 2-*N*-arylpyrrolecarbaldimino complexes. *Adv. Synth. Catal.* **2009**, *351*, 2625–2632. [CrossRef]
18. Mannam, S.; Alamsetti, S.K.; Sekar, G. Aerobic, Chemoselective oxidation of alcohols to carbonyl compounds catalyzed by a DABCO-copper complex under mild conditions. *Adv. Synth. Catal.* **2007**, *349*, 2253–2258. [CrossRef]
19. Marko, I.E.; Gautier, A.; Dumeunier, R.; Philippart, F.; Brown, S.M.; Urch, C.J. Efficient, Copper-catalyzed, aerobic oxidation of primary alcohols. *Angew. Chem. Int. Ed.* **2004**, *43*, 1588–1591. [CrossRef] [PubMed]
20. Hoover, J.M.; Stahl, S.S. Highly Practical Copper(I)/TEMPO Catalyst system for chemoselective aerobic oxidation of primary alcohols. *J. Am. Chem. Soc.* **2011**, *133*, 16901–16910. [CrossRef] [PubMed]
21. Steves, J.E.; Preger, Y.; Martinelli, J.R.; Welch, J.C.; Root, T.W.; Hawkins, J.M.; Stahl, S.S. Process development of Cu^{I}/ABNO/NMI-catalyzed aerobic alcohol oxidation. *Org. Process Res. Dev.* **2015**, *19*, 1548–1553. [CrossRef]
22. Wang, L.Y.; Bie, Z.X.; Shang, S.S.; Lv, Y.; Li, G.S.; Niu, J.Y.; Gao, S. Bioinspired aerobic oxidation of alcohols with a bifunctional ligand based on bipyridine and TEMPO. *RSC Adv.* **2016**, *6*, 35008. [CrossRef]
23. Markó, I.E.; Giles, P.R.; Tsukazaki, M.; Brown, S.M.; Urch, C.J.; Galano, A. Copper-catalyzed oxidation of alcohols to aldehydes and ketones: an efficient, aerobic alternative. *Science* **1996**, *274*, 2044–2046. [CrossRef] [PubMed]
24. Markó, I.E.; Gautier, A.; Mutonkole, J.-L.; Dumeunier, R.; Ates, A.; Urch, C.J.; Brown, S.M. Neutral, non-racemising, catalytic aerobic oxidation of alcohols. *J. Organomet. Chem.* **2001**, *624*, 344–347. [CrossRef]
25. Betzemeier, B.; Cavazzini, M.; Quici, S.; Knochel, P. Copper-catalyzed aerobic oxidation of alcohols under fuorous biphasic conditions. *Tetrahedron Lett.* **2000**, *41*, 4343–4346. [CrossRef]
26. Steves, J.E.; Stahl, S.S. Copper(I)/ABNO-catalyzed aerobic alcohol oxidation: Alleviating steric and electronic constraints of Cu/TEMPO catalyst systems. *J. Am. Chem. Soc.* **2013**, *135*, 15742–15745. [CrossRef] [PubMed]
27. Ryland, B.L.; Stahl, S.S. Practical aerobic oxidations of alcohols and amines with homogeneous copper/TEMPO and related catalyst systems. *Angew. Chem. Int. Ed.* **2014**, *53*, 8824–8838. [CrossRef] [PubMed]
28. Rafiee, M.; Miles, K.C.; Stahl, S.S. Electrocatalytic alcohol oxidation with TEMPO and bicyclic nitroxyl derivatives: Driving force trumps steric effects. *J. Am. Chem. Soc.* **2015**, *137*, 14751–14757. [CrossRef] [PubMed]
29. Zhang, G.F.; Han, X.W.; Luan, Y.X.; Wang, Y.; Wen, X.; Ding, C.R. L-Proline: an efficient *N*,*O*-bidentate ligand for copper-catalyzed aerobic oxidation of primary and secondary benzylic alcohols at room temperature. *Chem. Commun.* **2013**, *49*, 7908–7910. [CrossRef] [PubMed]
30. Sheldon, R.A. Recent advances in green catalytic oxidations of alcohols in aqueous media. *Catal. Today* **2015**, *247*, 4–13. [CrossRef]
31. Hoover, J.M.; Ryland, B.L.; Stahl, S.S. Mechanism of copper(I)/TEMPO-catalyzed aerobic alcohol oxidation. *J. Am. Chem. Soc.* **2013**, *135*, 2357–2367. [CrossRef] [PubMed]
32. Ryland, B.L.; McCann, S.D.; Brunold, T.C.; Stahl, S.S. Mechanism of alcohol oxidation mediated by copper(II) and nitroxyl radicals. *J. Am. Chem. Soc.* **2014**, *136*, 12166–12173. [CrossRef] [PubMed]
33. Rabeah, J.; Bentrup, U.; Stößer, R.; Brückner, A. Selective alcohol oxidation by a copper TEMPO catalyst: mechanistic insights by simultaneously coupled operando EPR/UV-Vis/ATR-IR spectroscopy. *Angew. Chem. Int. Ed.* **2015**, *127*, 11791–11794. [CrossRef] [PubMed]
34. Harvey, J.N.; Aschi, M.; Schwarz, H.; Koch, W. The singlet and triplet states of phenyl cation. A hybrid approach for locating minimum energy crossing points between non-interacting potential energy surfaces. *Theor. Chem. Acc.* **1998**, *99*, 95–99. [CrossRef]
35. Harvey, J.N.; Aschi, M. Spin-forbidden dehydrogenation of methoxy cation: A statistical view. *Phys. Chem. Chem. Phys.* **1999**, *1*, 5555–5563. [CrossRef]

36. Poli, R.; Harvey, J.N. Spin forbidden chemical reactions of transition metal compounds. New ideas and new computational challenges. *Chem. Soc. Rev.* **2003**, *32*, 1–8. [CrossRef] [PubMed]
37. Kozuch, S.; Shaik, S. How to conceptualize catalytic cycles? The energetic span model. *Acc. Chem. Res.* **2011**, *44*, 101–110. [CrossRef] [PubMed]
38. Kozuch, S. A refinement of everyday thinking: The energetic span model for kinetic assessment of catalytic cycles. *WIREs Comput. Mol. Sci.* **2012**, *2*, 795–815. [CrossRef]
39. Kozuch, S.; Sason, S. A combined kinetic-quantum mechanical model for assessment of catalytic cycles: application to cross-coupling and heck reactions. *J. Am. Chem. Soc.* **2006**, *128*, 3355–3365. [CrossRef] [PubMed]
40. Kozuch, S.; Shaik, S. Kinetic-quantum chemical model for catalytic cycles: The Haber-Bosch process and the effect of reagent concentration. *J. Phys. Chem. A* **2008**, *112*, 6032–6041. [CrossRef] [PubMed]
41. Uhe, A.; Kozuch, S.; Shaik, S. Software news and update automatic analysis of computed catalytic cycles. *J. Comput. Chem.* **2010**, *2011*, 978–985.
42. Lu, T.; Chen, F.W. Multiwfn: A multifunctional wavefunction analyzer. *J. Comput. Chem.* **2012**, *33*, 580–592. [CrossRef] [PubMed]
43. Michel, C.; Belanzoni, P.; Gamez, P.; Reedijk, J.; Baerends, E.J. Activation of the C-H bond by electrophilic attack: Theoretical study of the reaction mechanism of the aerobic oxidation of alcohols to aldehydes by the Cu(bipy)$^{2+}$/2,2,6,6-Tetramethylpiperidinyl-1-oxy cocatalyst system. *Inorg. Chem.* **2009**, *48*, 11909–11920. [CrossRef] [PubMed]
44. Belanzoni, P.; Michel, C.; Baerends, E.J. Cu(bipy)$^{2+}$/TEMPO-catalyzed oxidation of alcohols: Radical or nonradical mechanism? *Inorg. Chem.* **2011**, *50*, 11896–11904. [CrossRef] [PubMed]
45. Varela-Álvarez, A.; Liebeskind, L.S.; Musaev, D.G. Mechanistic insights into the aerobic copper(I)-catalyzed cross-coupling of S-Acyl thiosalicylamide thiol esters and boronic acids. *Organometallics* **2012**, *31*, 7958–7968. [CrossRef] [PubMed]
46. Frisch, M.J.; Trucks, G.W.; Schlegel, H.B.; Scuseria, G.E.; Robb, M.A.; Cheeseman, J.R.; Scalmani, G.; Barone, V.; Mennucci, B.; Petersson, G.A.; et al. *Gaussian 09, Revision C.01*; Gaussian, Inc.: Wallingford, CT, USA, 2010.
47. Becke, A.D. Density-functional thermochemistry. III. The role of exact exchange. *J. Chem. Phys.* **1993**, *98*, 5648–5652. [CrossRef]
48. Lee, C.; Yang, W.; Parr, R.G. Development of the Colic-Salvetti correlation-energy formula into a functional of the electron density. *Phys. Rev. B Condens. Matter* **1988**, *37*, 785–789. [CrossRef] [PubMed]
49. Becke, A.D. Density-functional exchange-energy approximation with correct asymptotic behavior. *Phys. Rev. A Gen. Phys.* **1988**, *38*, 3098–3100. [CrossRef] [PubMed]
50. Fukui, K. The path of chemical reactions-The IRC approach. *Acc. Chem. Res.* **1981**, *14*, 363–368. [CrossRef]
51. Fukui, K. A Formulation of the reaction coordinate. *J. Phys. Chem.* **1970**, *74*, 4161–4163. [CrossRef]
52. Lu, G.; Fang, C.; Xu, T.; Dong, G.B.; Liu, P. Computational study of Rh-catalyzed carboacylation of olefins: Ligand-promoted rhodacycle isomerization enables regioselective C−C bond functionalization of benzocyclobutenones. *J. Am. Chem. Soc.* **2015**, *137*, 8274–8283. [CrossRef] [PubMed]
53. Dang, Y.F.; Qu, S.L.; Tao, Y.; Deng, X.; Wang, Z.X. Mechanistic insight into ketone α-alkylation with unactivated olefins via C−H activation promoted by metal-organic cooperative catalysis (MOCC): Enriching the MOCC chemistry. *J. Am. Chem. Soc.* **2015**, *137*, 6279–6291. [CrossRef] [PubMed]
54. Bartoszewicz, A.; Miera, G.G.; Marcos, R.; Norrby, P.-O.G.; Martın-Matute, B. Mechanistic studies on the alkylation of amines with alcohols catalyzed by a bifunctional iridium complex. *ACS Catal.* **2015**, *5*, 3704–3716. [CrossRef]
55. Herbert, M.B.; Suslick, A.; Liu, P.; Zou, L.; Dornan, P.K.; Houk, K.N.; Grubbs, R.H. Cyclometalated c with modified N-chelating groups. *Organometallics* **2015**, *34*, 2858–2869. [CrossRef]
56. Luis, S.; Jonathan, M.G. How reliable are DFT transition structures? Comparison of GGA, hybrid-meta-GGA and meta-GGA functionals. *Org. Biomol. Chem.* **2011**, *9*, 689–700. [CrossRef]
57. Cannon, J.S.; Zou, L.; Liu, P.; Lan, Y.; O'Leary, D.J.; Houk, K.N.; Grubbs, R.H. Carboxylate-assisted C(sp^3)−H activation in olefin metathesis-relevant ruthenium complexes. *J. Am. Chem. Soc.* **2014**, *136*, 6733–6743. [CrossRef] [PubMed]
58. Hong, X.; Liang, Y.; Houk, K.N. Mechanisms and origins of switchable chemoselectivity of Ni-catalyzed C(aryl)−O and C(acyl)−O activation of aryl esters with phosphine ligands. *J. Am. Chem. Soc.* **2014**, *136*, 2017–2025. [CrossRef] [PubMed]

59. Dang, Y.; Qu, S.; Wang, Z.-X.; Wang, X. A Computational Mechanistic study of an unprecedented Heck-type relay reaction: insight into the origins of regio- and enantioselectivities. *J. Am. Chem. Soc.* **2014**, *136*, 986–998. [CrossRef] [PubMed]
60. Yang, Y.; Liu, P. Mechanism and origins of selectivities in the copper-catalyzed dearomatization-induced ortho C−H cyanation of vinylarenes. *ACS Catal.* **2015**, *5*, 2944–2951. [CrossRef]
61. Williams, T.J.; Bray, J.T.W.; Lake, B.R.M.; Willans, C.E.; Rajabi, N.A.; Ariafard, A.; Manzini, C.; Bellina, F.; Whitwood, A.C.; Fairlamb, I.J.S. Mechanistic elucidation of the arylation of non-spectator *N*-heterocyclic carbenes at copper using a combined experimental and computational approach. *Organometallics* **2015**, *34*, 3497–3507. [CrossRef]
62. Zhao, G.M.; Liu, H.L.; Zhang, D.D.; Huang, X.R.; Yang, X. DFT Study on Mechanism of *N*-Alkylation of Amino Derivatives with Primary Alcohols Catalyzed by Copper(II) Acetate. *ACS Catal.* **2014**, *4*, 2231–2240. [CrossRef]
63. Ariafard, A.; Zarkoob, F.; Batebi, H.; Stranger, R.; Yates, B. DFT studies on the carboxylation of the C−H bond of heteroarenes by copper(I) complexes. *Organometallics* **2011**, *30*, 6218–6224. [CrossRef]
64. Deng, X.; Dang, Y.F.; Wang, Z.X.; Wang, X.T. How does an earth-abundant copper-based catalyst achieve anti-Markovnikov hydrobromination of alkynes? A DFT Mechanistic Study. *Organometallics* **2016**, *35*, 1923–1930. [CrossRef]
65. Zhao, Y.; Truhlar, D.G. The M06 suite of density functionals for main group thermochemistry, thermochemical kinetics, noncovalent interactions, excited states, and transition elements: Two new functionals and systematic testing of four M06-class functionals and 12 other functionals. *Theor. Chem. Account.* **2008**, *120*, 215–241. [CrossRef]
66. Zhao, Y.; Truhlar, D.G. Density functionals with broad applicability in chemistry. *Acc. Chem. Res.* **2008**, *41*, 157–167. [CrossRef] [PubMed]
67. Marenich, A.V.; Cramer, C.J.; Truhlar, D.G. Universal solvation model based on solute electron density and on a continuum model of the solvent defined by the bulk dielectric constant and atomic surface tensions. *J. Phys. Chem. B* **2009**, *113*, 6378–6396. [CrossRef] [PubMed]
68. Kruse, H.; Grimme, S. A geometrical correction for the inter- and intra-molecular basis set superposition error in Hartree-Fock and density functional theory calculations for large systems. *J. Chem. Phys.* **2012**, *136*, 154101–154116. [CrossRef] [PubMed]
69. Brandenburg, J.G.; Alessio, M.; Civalleri, B.; Galano, A.; Peintinger, M.F.; Bredow, T.; Grimme, S. Geometrical correction for the inter- and intramolecular basis set superposition error in periodic density functional theory calculations. *J. Phys. Chem. A* **2013**, *117*, 9282–9292. [CrossRef] [PubMed]
70. Grimme, S.; Antony, J.; Ehrlich, S.; Krieg, H. A consistent and accurate ab initio parametrization of density functional dispersion correction (DFT-D) for the 94 elements H-Pu. *J. Chem. Phys.* **2010**, *132*, 154104–154123. [CrossRef] [PubMed]
71. Grimme, S. Semiempirical GGA-Type density functional constructed with a long-range dispersion correction. *J. Comput. Chem.* **2006**, *27*, 1787–1799. [CrossRef] [PubMed]
72. Grimme, S. Accurate Description of van der Waals complexes by density functional theory including empirical corrections. *J. Comput. Chem.* **2004**, *25*, 1463–1473. [CrossRef] [PubMed]
73. Hoffmann, A.; Grunzke, R.; Herres-Pawlis, S. Insights into the influence of dispersion correction in the theoretical treatment of guanidine-quinoline copper(I) Complexes. *J. Comput. Chem.* **2014**, *35*, 1943–1950. [CrossRef] [PubMed]
74. Sousa, S.F.; Pinto, G.R.; Ribeiro, A.J.M.; Coimbra, J.T.S.; Fernandes, P.A.; Ramos, M. Comparative analysis of the performance of commonly available density functionals in the determination of geometrical parameters for copper complexes. *J. Comput. Chem.* **2013**, *34*, 2079–2090. [CrossRef] [PubMed]
75. Chai, J.-D.; Head-Gordon, M. Long-range corrected hybrid density functionals with damped atom-atom dispersion corrections. *Phys. Chem. Chem. Phys.* **2008**, *10*, 6615–6620. [CrossRef] [PubMed]
76. Yury, M.; Åsmund, S.; Giovanni, O. The accuracy of DFT-optimized geometries of functional transition metal compounds: A validation study of catalysts for olefin metathesis and other reactions in the homogeneous phase. *Dalton Trans.* **2012**, *41*, 5526–5541. [CrossRef]
77. Mouesca, J.M.; Mouesca, J.-P.; Noodleman, L.; Bashford, D.; Case, D.A. Density functional Poisson-Boltzmann calculations of redox potentials for iron-sulfur clusters. *J. Am. Chem. Soc.* **1994**, *116*, 11898–11914. [CrossRef]

78. Noodleman, L. Valence bond description of antiferromagnetic coupling in transition metal dimers. *J. Chem. Phys.* **1981**, *74*, 5737–5743. [CrossRef]
79. Ciofini, L.; Daul, C.A. DFT calculations of molecular magnetic properties of coordination compounds. *Coord. Chem. Rev.* **2003**, *238*, 187–209. [CrossRef]
80. Siegbahn, P.E.M.; Pelmenschikov, V. Nickel superoxide dismutase reaction Mechanism Studied by Hybrid Density Functional Methods. *J. Am. Chem. Soc.* **2006**, *128*, 7466–7475. [CrossRef]
81. Bassan, A.; Blomberg, M.R.A.; Siegbalm, P.E.M.; Que, L. A density functional study on a biomimetic non-heme iron catalyst: insights into alkane hydroxylation by a formally HO-Fe^{V}=O oxidant. *Chem. Eur. J.* **2005**, *11*, 692–705. [CrossRef] [PubMed]
82. Bachler, V.; Chaudhuri, P.; Wieghardt, K. The symmetry-broken formalism applied to the electronic structure of an iminosemiquinone copper(II) catalyst: A key to the qualitative understanding of its reactivity. *Chem. Eur. J.* **2001**, *7*, 404–415. [CrossRef]
83. Cheng, L.; Li, J.; Zhang, Q.C.; Ma, L.S.; Yang, J.C. DFT studies on the mechanism of alcohol oxidation by the (bpy)Cu^{I}-TEMPO/NMI catalytic system. *Dalton Trans.* **2015**, *44*, 7395–7403. [CrossRef] [PubMed]